

# A physics-based earthquake simulator replicates seismic hazard statistics across California

Bruce E. Shaw<sup>1\*</sup>, Kevin R. Milner<sup>2</sup>, Edward H. Field<sup>3</sup>, Keith Richards-Dinger<sup>4</sup>,  
Jacquelyn J. Gilchrist<sup>2</sup>, James H. Dieterich<sup>4</sup>, Thomas H. Jordan<sup>2</sup>

Seismic hazard models are important for society, feeding into building codes and hazard mitigation efforts. These models, however, rest on many uncertain assumptions and are difficult to test observationally because of the long recurrence times of large earthquakes. Physics-based earthquake simulators offer a potentially helpful tool, but they face a vast range of fundamental scientific uncertainties. We compare a physics-based earthquake simulator against the latest seismic hazard model for California. Using only uniform parameters in the simulator, we find strikingly good agreement of the long-term shaking hazard compared with the California model. This ability to replicate statistically based seismic hazard estimates by a physics-based model cross-validates standard methods and provides a new alternative approach needing fewer inputs and assumptions for estimating hazard.

## INTRODUCTION

Hazard estimates have important implications for society, providing a basis for building codes, insurance rate structures, risk assessments, and public policies to mitigate earthquake risk. The basic structure of methods for estimating hazard was developed by engineers needing quantitative answers despite the wide range of uncertainties (1). The method, Probabilistic Seismic Hazard Analysis (PSHA), relies on parameterized statistical models combining long-term earthquake event fault rupture probabilities and ground motion models (GMMs) of shaking for the events. Recent advances in PSHA rupture models now allow for the possibility of multifault ruptures (2), something often seen in large complex earthquakes [for example, the 1992  $M$  (magnitude) 7.1 Landers (3), 2001  $M$  7.8 Kunlun (4), 2002  $M$  7.9 Denali (5), and 2016  $M$  7.8 Kaikoura (6) events]. However, these extensions have only added to the complexity and assumptions underlying the models. Indeed, the complexity of PSHA models, the difficulty in testing them, the paucity of calibration data, and the consequent uncertainties in the parameters have led to persistent controversies regarding the utility and accuracy of the whole exercise (7–9). A recent critique by Mulargia *et al.* (9) is categorical: “PSHA rests on assumptions now known to conflict with earthquake physics.... PSHA is fundamentally flawed and should therefore be abandoned.”

Here, we take a new approach to this problem, based on the use of a physics-based earthquake simulator to generate a region-specific set of earthquake ruptures that are self-consistent with specified physics properties. The idea was that this could complement the PSHA by greatly reducing uncertain inputs, scaling statistics, and assumptions that are pieced together in current hazard models. We report here on a result found in our initial efforts at comparing the hazard coming from the simulator and the latest state-of-the-art California earthquake rupture forecast, UCERF3 (Uniform California Earthquake Rupture Forecast, version 3), which forms the basis for the California component of the National Seismic Hazard Model developed by the U.S. Geological Survey (USGS) (10). Using GMMs to map the rup-

ture sets onto shaking hazard, we find remarkable agreement on a series of hazard measures of deep engineering interest. This includes standard hazard measures of ground acceleration shown in the national hazard maps and close agreement extending over broader probability levels and spectral shaking periods. The replication of the statistical UCERF3 hazard model by a physics-based model provides a strongly increased confidence in the hazard estimates through triangulation using very different methods (11) and a new tool for understanding its origins and robustness. It also provides a new method for estimating hazard needing fewer inputs and assumptions.

## The models

The models are very different. The UCERF3 model continues a long line of seismic hazard models that link together a series of empirical regressions and scaling laws to estimate hazard in a statistical manner. The UCERF3 model provides a number of important advances to the traditional methods, in particular relaxing the fault segmentation hypotheses to allow faults to break partially and together, enabling a vastly more complex set of ruptures. There are a large number of parameters in the model, and a huge number of logic tree branches, representing model uncertainties, with branch weights set by expert opinion. It has been developed with increasing levels of time-dependent sophistication, beginning with the time-independent model focused on long-term hazard (2). The current state of the time-dependent hazard given both the recency of the last earthquake rupture on a fault and the time-dependent recovery of elastic stresses was addressed by the UCERF3-TD (time-dependent) model (12). The most recent version addresses a major issue of spatial and temporal clustering and the large changes in probabilities associated with aftershocks (13), although also at a cost of increased model complexity.

The core engine of the physics-based simulator model is the RSQSim platform (14, 15). It is a boundary element model using three key approximations. First, elements interact with quasistatic elastic interactions, so dynamic stresses are neglected. Second, rate-and-state frictional behavior is simplified into a three-regime system where elements are either stuck, nucleating, or sliding dynamically. Third, during dynamic sliding, slip rate is fixed at a constant sliding rate. These approximations allow for analytic treatments of rate-and-state behaviors in different sliding regimes, allowing adaptive time stepping needed only for state changes and a tremendous speedup computationally.

Copyright © 2018  
The Authors, some  
rights reserved;  
exclusive licensee  
American Association  
for the Advancement  
of Science. No claim to  
original U.S. Government  
Works. Distributed  
under a Creative  
Commons Attribution  
NonCommercial  
License 4.0 (CC BY-NC).

<sup>1</sup>Lamont Doherty Earth Observatory, Columbia University, Palisades, NY 10025, USA. <sup>2</sup>Department of Earth Science, University of Southern California, Los Angeles, CA 90089, USA. <sup>3</sup>U.S. Geological Survey, Golden, CO 80401, USA. <sup>4</sup>Department of Earth Science, University of California Riverside, Riverside, CA 92521, USA.  
\*Corresponding author. Email: shaw@ldeo.columbia.edu

Richards-Dinger and Dieterich (15) have presented a number of favorable comparisons of this model with fully dynamic simulations and observations, although they are, of course, not equivalent. The main features of the rate-and-state equations are preserved, leading to delayed nucleation and other effects in which clustering of events arises naturally and appears realistic when compared with earthquake observations. The model produces an emergent deterministic complex sequence of events starting from initial conditions. The common beginning point inputs to the simulator and hazard model were the UCERF3 fault system and the geologically determined slip rates on faults. The version of the simulator that we use here and that is applied to the UCERF3 fault system uses a new hybrid loading technique, which combines traditional backslip methods that fix the faults to slip at a given rate with a remote loading at a fixed stressing rate (16) to now give a hybrid stressing rate that reduces fault end and edge sensitivities in the original version. More details of the loading are contained toward the end of the paper in the “Hybrid loading” section.

As an initial effort, we built a baseline case out of geologically and geodetically determined faults and slip rates and uniform global model frictional parameters. The only tuning was to have the few free model parameters tuned, again globally and uniformly, so as to match observed earthquake scaling relations. The goals of this tuning were to match slip as a function of earthquake size for large events (2, 17) and to yield a frequency distribution of moderate-sized events with a Gutenberg-Richter  $b$  value close to 1. The hybrid loading technique aided in these matches and resulted in better agreement with the observed depth dependence of seismicity. Rate-and-state friction parameters  $a = 0.001$  and  $b = 0.008$ , a normal stress of 100 MPa, a fault depth of 18 km with seismogenic loading from 2 to 14 km, and equilateral triangles with a grid resolution of 1.8 km on a side formed a baseline case.

A second stage in the modeling was anticipated, whereby model behaviors would be adjusted locally using location-specific adjustments to bring the simulator behaviors closer to the hazard model estimates, much as “flux corrections” have been used in climate models to adjust model behaviors to be closer to desired states. Before proceeding to this sizable free-parameter adjustment phase, we looked at various metrics relevant to hazard to see how different the baseline uniform model was from the UCERF3 model. We report here the finding that the baseline uniform simulator models show surprisingly good agreement with the hazard models on a number of important hazard metrics without any local parameter tuning.

## RESULTS

### Comparison of the simulator with the hazard model

Figure 1 shows pointwise comparisons of hazard-relevant behaviors of the RSQSim simulator with UCERF3. Figure 1A shows the use of a measure of hazard-relevant behavior we first looked at to see whether the models were even in the same ballpark. We compare the mean interevent recurrence intervals for earthquakes above a given size in the UCERF3 hazard model and in the simulator. These recurrence intervals are calculated at the subsection scale in the UCERF3 California fault model, where subsections are subdivisions of faults of seismogenic width in the down-dip depth direction and half that length in the along-strike direction (2). The vertical axis shows measured repeat times at the element scale for the simulators, calculated by dividing the catalog length by the number of times the event ruptured in an event above a cutoff magnitude. The individual triangular elements have a corresponding fault subsection based on their approximate

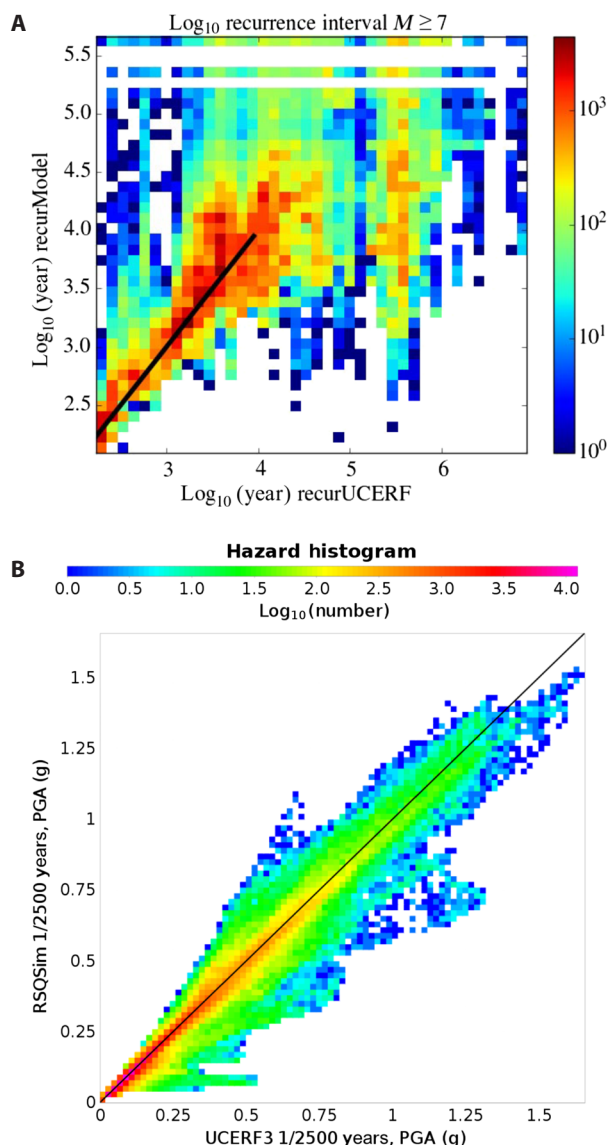


**Fig. 1. Hazard-relevant measures in the simulator compared with the UCERF3 hazard model.** (A) Recurrence intervals in the earthquake simulator compared with the UCERF3 hazard model. Plot shows a two-dimensional (2D) pointwise histogram of 265k elements on fault for  $M \geq 7$ . Color shows number in histogram. The diagonal solid black line shows what would be perfect agreement. The lower left part shows the fastest-moving areas of the fault system with the shortest recurrence intervals. The horizontal lines at the top show the finiteness of the catalog, with the top horizontal set being patches that have broken once during the catalog above the cutoff magnitude, the next horizontal set below having broken twice, and so on. (B) Pointwise shaking hazard in the simulator compared with UCERF3. This is for a standard hazard measure, 2% in 50 years peak ground acceleration (PGA). Plot shows 2D pointwise shaking hazard across California coming from  $M 6.5+$  events for the simulator events compared with on-fault UCERF3 events. Note that the hazard measure agrees even better than the recurrence intervals.

tiling of the UCERF3 fault subsections. They are not, however, exact reproductions of the UCERF3 subsections, as the faults have been tiled to be a smoother representation of the fault system, removing discontinuities that would arise from simple extrapolations of rectangular subsection scale patches to depth. Figure 1A plots a 2D histogram

with color representing log densities of points. The diagonal solid black line shows what would be perfect agreement. Figure 1A shows only the largest events, those above  $M 7$ . This initial favorable comparison led us to examine other measures with which to compare the simulator against UCERF3.

We chose to look at shaking hazard primarily because hazard is the measure we ultimately most wanted to know and, therefore, were most concerned with similarities and differences. Thus, we turned to a standard hazard measure, one used in the national seismic hazard maps, the PGA 2% exceedance in 50 years, which is the peak level of ground acceleration expected to be exceeded at the 2% probability level over a 50-year time period, or an annual probability of 1/2500 years, expressed as a fraction of the acceleration of gravity. We calculated this hazard for both models arising from on-fault  $M 6.5+$  events. We calculated the shaking hazard at regular map grid points using the model catalogs of finite ruptures together with statistical empirical

GMMs to obtain shaking levels for individual events given their magnitude and distance and other relevant features (such as focal mechanism). This was done using the OpenSHA platform (18). We applied the GMMs used in the national hazard maps [an average of the NGA-West2 model set (19)] with both UCERF3 and the simulator catalogs. To regularize the comparison, we mapped the RSQSim ruptures onto the UCERF3 fault subsections and then applied the GMMs to calculate hazard. While the RSQSim rupture sequences are deterministically generated, the GMMs add a stochastic element in estimating ground motions associated with the deterministic simulator events. Figure 1B shows pointwise comparison of this PGA hazard for the simulator compared with UCERF3. Note that the correspondence is even tighter for the hazard in Fig. 1B than for the recurrence intervals in Fig. 1A.

To illustrate the spatial correspondence, Fig. 2 shows maps of the hazard and differences. To put the comparisons in perspective, we also

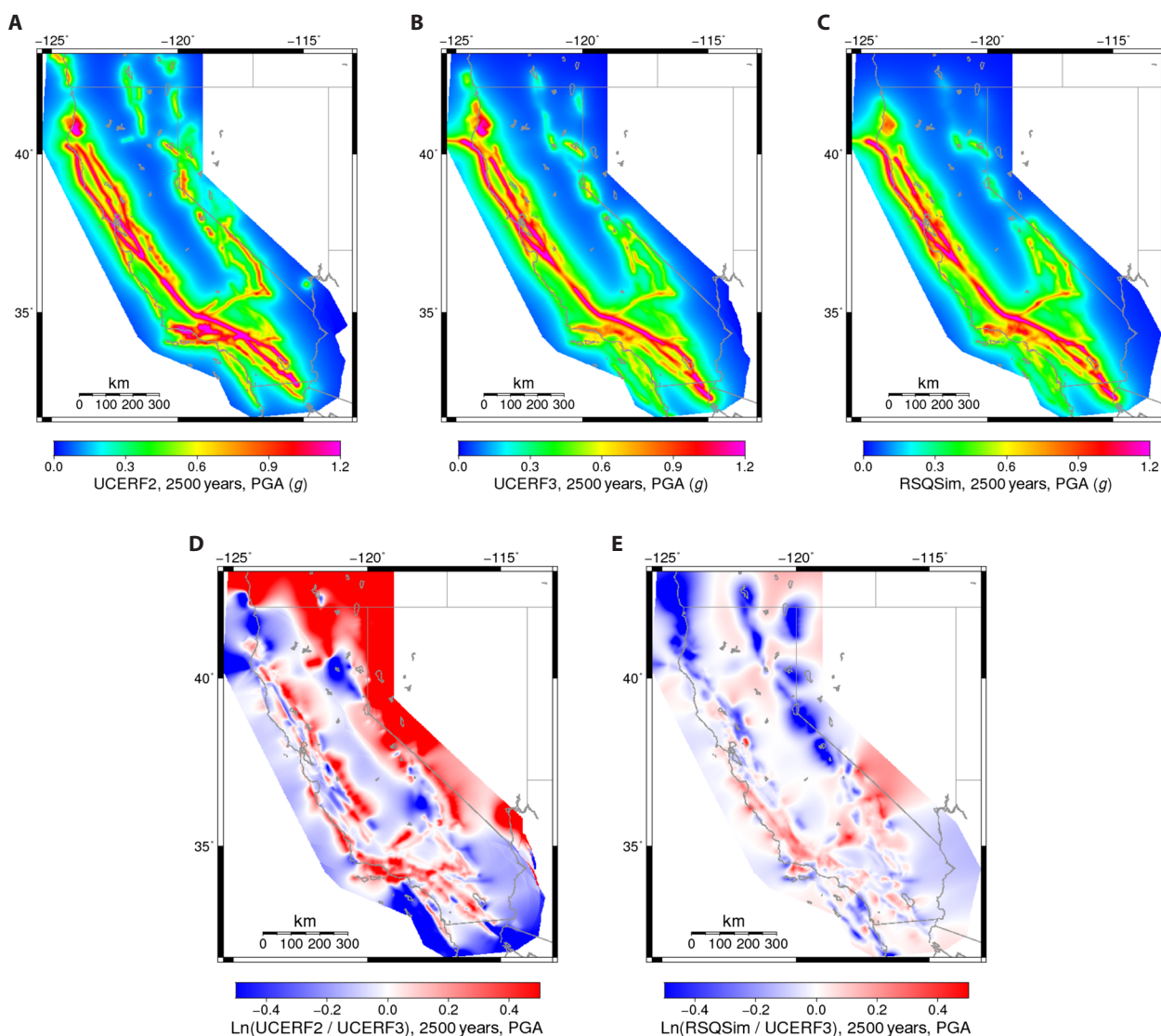


**Fig. 2. Maps of shaking hazard in the earthquake simulator compared with the UCERF3 hazard model and plots of differences.** The immediate predecessor UCERF2 California hazard model is shown for comparison. Maps show PGA 2% in 50-year exceedance. Units are in fractions of the acceleration of gravity  $g$ . (A) UCERF2. (B) UCERF3. (C) RSQSim model. (D) Map of  $\ln$  ratio of UCERF2/UCERF3 shaking hazard. (E) Map of  $\ln$  ratio of simulator/UCERF3 shaking hazard. Note that the simulator is even closer to UCERF3 than UCERF2 is to UCERF2.

show the previous hazard map, UCERF2. We see even closer correspondence between UCERF3 and the simulator than we do between UCERF3 and its immediate predecessor, UCERF2. Figure 2D shows a map of the natural log of the ratio of UCERF2 to UCERF3, and Fig. 2E shows a map of the natural log of the ratio of RSQSim to UCERF3, to better see the spatial pattern of the differences. Impressively, mean absolute natural log differences averaged across the state are only 0.10, corresponding to an average of only an 11% difference in PGA values for the simulator compared with UCERF3.

While PGA 2%/50-year hazard levels are a standard measure used in national seismic hazard maps and building codes, full hazard curves exploring more frequent lower ground motions and more rare extreme ground motions are also important. Critical facilities such as

hospitals and power plants, for example, are designed for more extreme ground motions. In Fig. 3, we plot a set of full hazard curves across a range of probabilities for several specific sites, for reasons of societal interest locations of cities taken from the National Earthquake Hazards Reduction Program set of California cities (20). The first plots are the largest cities in California by population (Los Angeles, San Diego, San Jose, and San Francisco), with two more cities added based on proximity to faulting types of interest—the San Andreas (San Bernardino) and the coastal thrust faults (Santa Barbara). We note impressive agreement across the range of probabilities, particularly at lower probabilities and more extreme ground motions. Differences at higher probabilities correspond to smaller, more frequent events. To capture this regime properly, we need to be able to go beyond

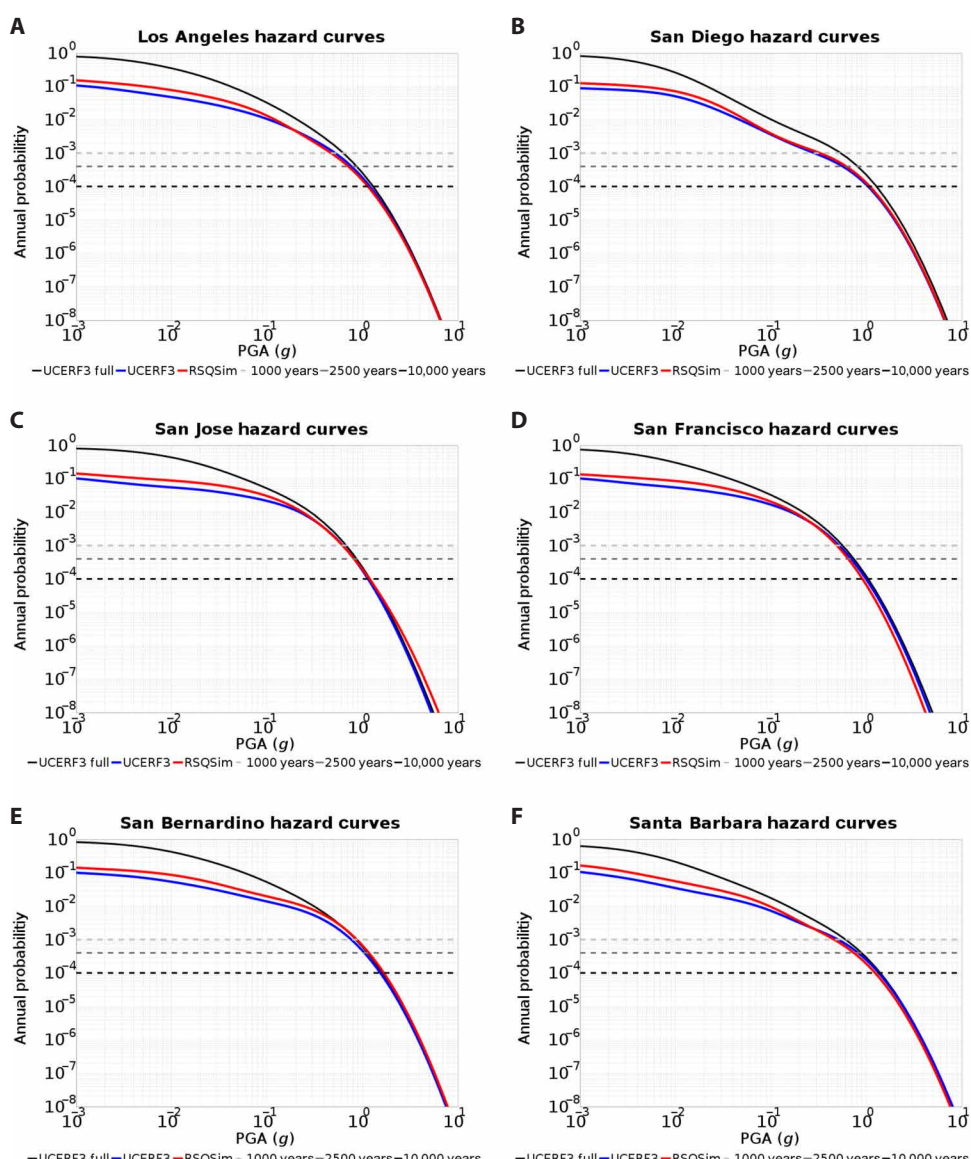


**Fig. 3. Full hazard curves for some example cities.** The first four cities are by largest population in California, and the next two are added as examples due to proximity to San Andreas and thrust faults. The horizontal axis is PGA as a fraction of gravity acceleration  $g$ . The vertical axis is annual probability of exceedance. Red lines show RSQSim results. Blue lines show UCERF3 results for on-fault events. Black lines show full UCERF3 hazard results for all events, including off-fault events, as reference to also show off-fault hazard that is not being included. Horizontal dashed line shows the 2500-year standard reference curve in the middle, the 1000-year curve on top, and the 10,000-year curve at the bottom. Cities are as follows: (A) Los Angeles, (B) San Diego, (C) San Jose, (D) San Francisco, (E) San Bernardino, and (F) Santa Barbara.

on-fault events and also capture off-fault events as well, corresponding to the background events in the UCERF3 model. This is an area for future development and study.

### Extending the comparison

Robustness of the agreement to measure and model details is another key aspect of replication. Finding agreement in PGA 2%/50-year probabilities led us to extend to a broader spectrum of probabilities, where we found continued agreement. Extending hazard measures from PGA to spectral measures at other longer periods, we can push the comparison further. Spectral acceleration  $PSA(T)$  for different periods  $T$  is a standard hazard measure of additional engineering interest, with PGA being a high-frequency limit of this measure.  $PSA(T)$ , or pseudo-spectral acceleration at period  $T$  seconds, is a measure of ground motion used by engineers to evaluate building response at a resonant period  $T$ . Larger structures have longer-period resonant responses, with a rule of thumb being 0.1 s per story. Different magnitude events emit different amounts of short- and long-period shaking motions, so studying different  $PSA(T)$  further extends the comparison, probing different magnitude and spatial aspects of the event distributions, using additional measures of engineering interest. Figure 4 shows a sweeping comparison of a full range of spectral periods and probabilities. Figure 4 shows the mean absolute difference in natural log hazard as a function of probability for different spectral periods. This is a useful metric in that it tracks ratios across a range of underlying values and penalizes equally for being either high or low. At a broad scale, we see impressive agreement at probability levels below time scales corresponding to repeat times of large events (hundreds of years), indicating agreement in long-term time-independent hazard. At time scales shorter than a few centuries, below the repeat times of large events where details concerning smaller events become important, the curves begin to diverge. We see excellent agreement in spectral acceleration  $PSA(T)$  across the engineering relevant band of  $T = 0.2$  to 1 s over probability levels of  $10^{-3}$  to  $10^{-5}$  year $^{-1}$ . At longer spectral periods,  $T = 5$  and 10 s, we again see excellent agreement at  $10^{-3}$  probability levels, as well as some deviations developing at the lowest probability levels sensitive to the largest events. Even then, however, mean absolute differences are still only a few tens of percent.

Turning to the question of sensitivity of the results to the model, we checked that the physics-based model results are not overly sensitive to parameters, by looking at small but finite changes in parameters and seeing that, within the model, changes in mean absolute log hazard measures are small; specifically, looking at changes in reference friction parameter values  $a$ ,  $b$ , and  $\sigma_n$  of up to  $\pm 25\%$ , we found less than 10% changes in long-term mean absolute hazard ratios. Details of sensitivity studies are presented in the Supplementary Materials.

The broad robust agreement of the different estimation methods on long-term hazard raises the question of what factors of the system contribute to this replicability. In part, some of the model differences in the spatial extent of ruptures are smoothed in the shaking hazard, as ruptures at different distances contribute to the hazard. In addition, the effect of differences in how precisely the models are choosing to break in different sized events is reduced somewhat through the complementarity of having fewer larger events with bigger mean shaking or more slightly smaller events with smaller mean shaking but more chances at higher ground motions. A further important feature that contributes to the robustness is the relative insensitivity of the GMMs to the magnitude at large magnitudes. Close to large events, shaking at high frequencies has only a weak dependence on

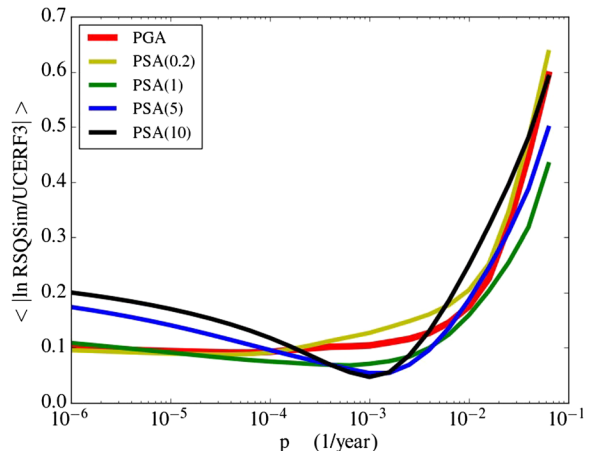


**Fig. 4. Good agreement in long-term hazard.** Averaging over the state, we plot mean absolute  $|\ln(\text{RSQSim}/\text{UCERF3})|$  as a function of probability level for different  $PSA(T)$ .  $PSA(T)$  at different resonant period  $T$  seconds is pseudo-spectral acceleration, a measure of ground motion used by engineers relevant to building response. Different curves are for different spectral periods  $T$ , shown with PGA (red), at  $T = 0.2$  s (yellow),  $T = 1$  s (green),  $T = 5$  s (blue), and  $T = 10$  s (black). Note the very good correspondence for long-term hazard at annual probabilities of  $p = 10^{-3}$  year $^{-1}$  and below, which are regions of central engineering importance. At time scales shorter than a few centuries, below the repeat times of large events where details concerning smaller events become important, the curves begin to diverge.

magnitude (21). This weak dependence reflects the fact that high-frequency ground motions decay rapidly with distance; thus, it is predominantly just the closest parts of the faults that contribute to the high-frequency shaking, and very large events that contain much more distant areas add little to this measure. At longer periods, there is more but still weak magnitude dependence for a given distance from large earthquakes. These weak magnitude dependencies reduce the hazard differences coming from detailed model magnitude distribution differences. A topic of further research is how different these measures could be given the input constraints of fault geometry and slip rate and event scaling, together with the application of GMMs to the output.

Figure 4 contains a lot of condensed information, so a disaggregation is useful to see what is underlying these curves. In Fig. 5, we plot the underlying hazard maps and difference plots for an example spectral acceleration at a set of return periods, specifically  $PSA(1)$  at 1000-, 2500-, and 10,000-year return periods. This translates into three points along one curve in Fig. 4, with each point being an average of the absolute value of the difference curve on the right panels in Fig. 5. By disaggregating things, we see that there is a lot of underlying spatial structure the simulator is managing to match with the hazard model, something that changes as longer return periods probe more features of the slower-moving faults. Replicating hazard across a wide range of time, space, and spectral periods is seen here to represent an information-rich achievement.

### Dominant magnitude

While a broadly successful replication has been achieved, there are some underlying differences in the distributions that can be seen to make a difference at some scales in some hazard measures. Looking at the events that dominate the net slip on faults helped illuminate one regime where differences mattered at the hazard scale. To do this,

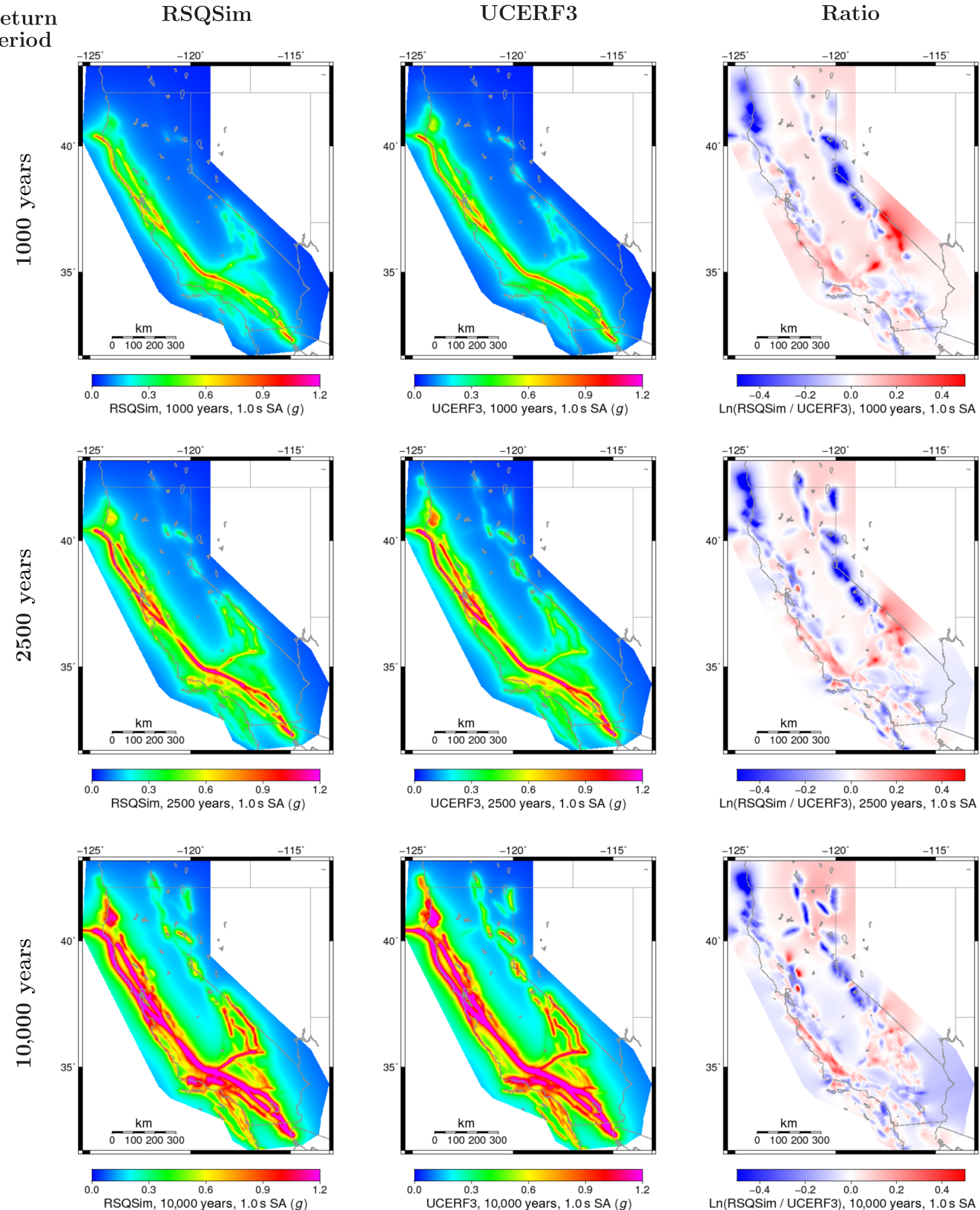


**Fig. 5. Maps of PSA(1) 1-s spectral acceleration shaking hazard in the earthquake simulator compared with the UCERF3 hazard model, and plots of differences, for different return periods.** Note the illumination of slower-moving faults at longer return periods and the good correspondence between the simulator and the hazard model across these changes.

we looked at the “dominant magnitude” on faults. This was defined by considering all the events a point on a fault participated in and identifying the largest magnitude in that distribution of sizes of events it participated in containing half or more of the cumulative moment at that magnitude and above, the participation cumulant moment median. This is a type of “corner” magnitude, measured in a nonparametric robust way. It is a new measure we introduce here, a useful one in examining large events. Figure 6 shows this measure for UCERF3 and the simulator. A key feature we see in the UCERF3 map of this quantity is the effect of the fault system linkage in UCERF3, where faults having a separation of <5 km were allowed to break together.

This rule manifests itself in the dominant magnitude of the system, as illustrated in the overlap between the linked fault cluster in Fig. 6C and the UCERF3-dominant magnitude in Fig. 6B. The simulator, in contrast, produces its own choices in a self-organizing way of how faults link up. Figure 6D shows a difference plot of dominant magnitude between the simulator and UCERF3. Systematic spatial differences are seen, with UCERF3 having larger dominant magnitudes along major faults and smaller dominant magnitudes along outlying minor faults. Figure 6E shows a hazard measure more sensitive to these dominant magnitude differences, the long-period PSA(10) at  $p = 10^{-4}$  year $^{-1}$ . [This is in contrast to the shorter-period PGA shown

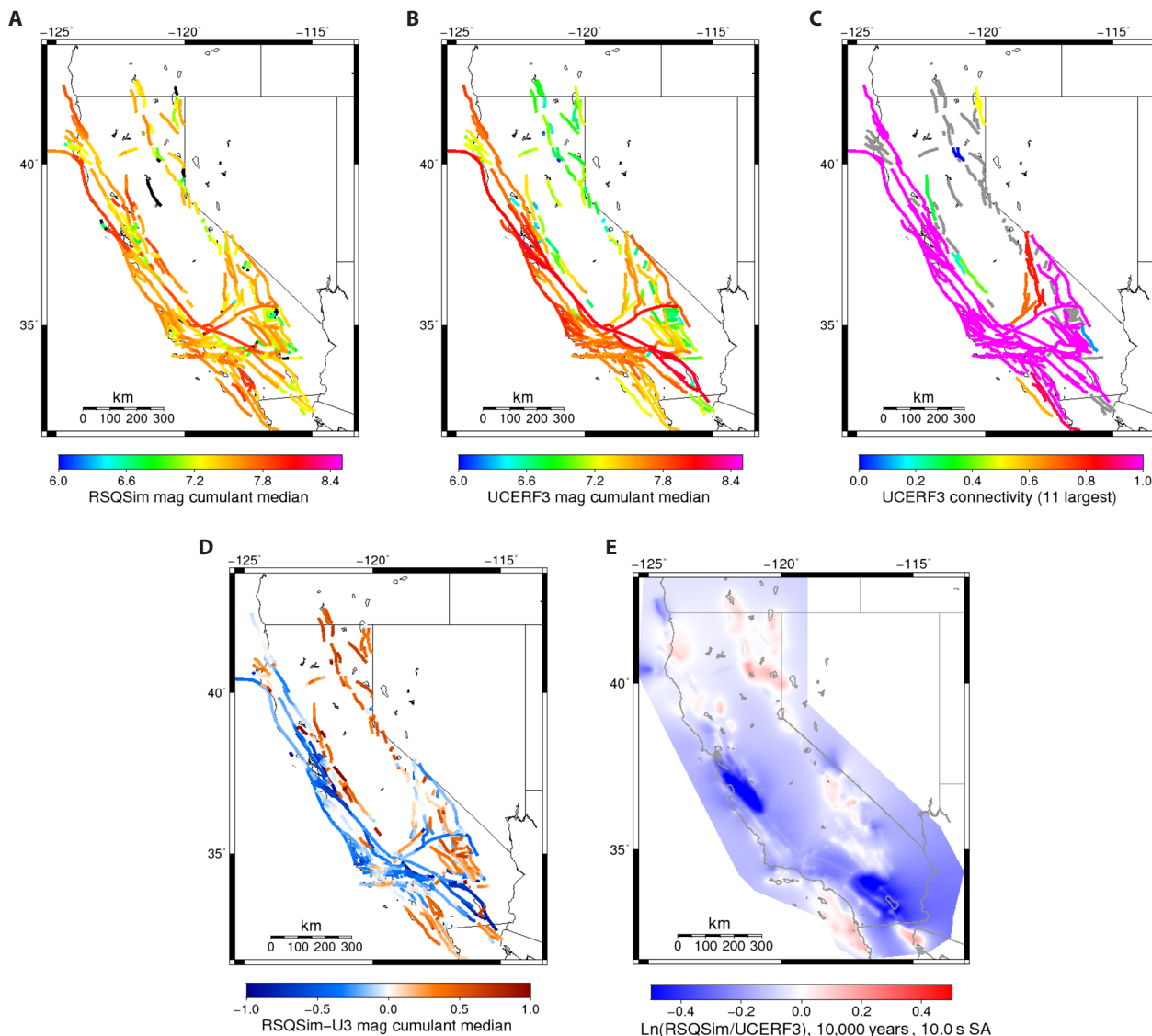


**Fig. 6. Dominant magnitude.** Maps of dominant magnitude in the earthquake simulator compared with UCERF3, relationship with UCERF3 fault linkage rules, and impact on long-period hazard. (A) Simulator. (B) UCERF3. (C) UCERF3 fault system connectivity. Colors show connected clusters, with colors indicating cluster sizes in rank order from magenta (largest) to blue (smallest), with only the largest 11 clusters shown. The underlying colors are thus not continuous but a discrete rank ordering. Note that the dominant magnitude in UCERF3 correlates closely with the largest cluster. (D) Difference in dominant magnitude simulator–UCERF3. Note that, on the major faults, UCERF3 tends to have larger dominant magnitudes, whereas on the minor outlying faults, the reverse occurs. The color here shows magnitude difference. (E) Map of long-period long-term hazard difference, showing  $\ln(\text{simulator}/\text{UCERF3})$  of PSA(10) at  $p = 10^{-4}$  year $^{-1}$ , a measure for which dominant magnitude differences are expected to have more of an impact. Note that the two areas with substantial dominant magnitude differences of order unity on major faults, around the San Francisco Bay Area and in the Southern San Andreas and San Jacinto fault area, are the two areas that show substantial hazard differences. Otherwise, the hazard differences are modest.

in Fig. 2E and PSA(1) in Fig. 5, which are less sensitive to these dominant magnitude differences.] In Fig. 6E, we see significant PSA(10) hazard differences emerging, where strong dominant magnitude differences of order unity on fast-moving major faults occur in the San Francisco Bay Area and at the Southern San Andreas San Jacinto fault areas, but aside from these areas, differences are typically modest.

## DISCUSSION AND CONCLUSION

We have found remarkable robust agreement between statistical and physics-based models for hazard measures of central engineering interest. These include PGA and PSA from 0.2 to 1 s, at  $10^{-3}$  to  $10^{-5}$  annual probability levels, which include much of the realms upon which building codes are based. Replication of long-term seismic hazard coming from two very different approaches—a form of triangulation (11), with one approach using a more traditional statistical method and the other one using a new physics-based simulator method—provides an important cross-validation and increased confidence in our ability to estimate values of these societally important quantities. It also offers a new tool that needs fewer inputs and assumptions for estimating long-term seismic hazard.

## MATERIALS AND METHODS

The main hazard results have been presented. Here, we present some additional model details. The hybrid loading approach we introduce below is a new method that improves a number of simulator behaviors.

### Seismogenic depth

While UCERF3 used spatially varying seismogenic depths, on the basis of the 95% contour of background seismicity, we chose to use a uniform seismogenic depth on all the faults in the simulator. This was done for a number of reasons. First, the degree to which dynamic ruptures can rupture coseismically below the seismogenic depth is an open question (22, 23). Second, the step changes in seismogenic depth in UCERF3 are likely oversimplified and, yet, may affect the behavior by creating discontinuities. Looking to build the simplest model first, we thus chose a uniform depth. Examining sensitivity to this depth is an example of the types of epistemic uncertainties we can explore in this framework.

### Hybrid loading

The method of hybrid loading is meant to tie faults to target long-term slip rates but then load them gently in a way that does not overforce them to slip in ways they would rather not, as they are ultimately self-organizing systems (24). Traditional backslip methods that load at a constant slip rate along a fault and to the base of the seismogenic depth create stressing rate singularities at the base and ends and then generate many small events at those edges that try to fill in the imposed long-term slip-rate profile. Here, we aim to recreate the long-term slip rates along the bulk of the fault but add gentler stress-rate loading to accomplish this. The procedure is as follows:

(1) Begin with a target slip rate. Typically, this is taken to be a constant along strike and with depth, but if further information is available to modify this, other slip profiles can be used.

(2) Calculate what the stressing rates would be for the fault system loaded in backslip mode with this slip-rate profile.

(3) Smooth and modify the backslip-estimated stressing rates. This is done with a series of filters.

(i) Add upper and lower unstressed layers to represent the non-seismogenic layers. On the top  $Z_1$  km and bottom  $Z_2$  km in depth, the shear stressing rate is zeroed out. This is done to get things loading and nucleating in the seismogenic middle zone. A physical justification is the lower-modulus upper layer and the higher-temperature creep relaxation processes in the lower layer. The effect in the simulator is to improve the depth dependence of the hypocenters.

(ii) Correct the stressing rate by  $1/(H - Z_1 - Z_2)$  to maintain the overall slip rate on the fault, where  $H$  is the fault depth. An additional multiplicative factor may be needed in the case of initial slip profiles, such as constant slip with depth, which have nonuniform depth dependence. An overall multiplicative factor correcting stressing rates can be added at this stage. For the case ( $H = 18$  km,  $Z_1 = 2$  km, and  $Z_2 = 4$  km) we will be using in our model, a factor of 1.2 was seen to give a good match to slip rates.

(iii) On  $Z_3$ -km-wide edges, take the median stressing rate for that fault depth and extend it to the sides. This gets rid of fault edge singularities. (In our case, we use  $Z_3 = 5$  km.) It also allows the fault slip to taper at the edges in a self-organizing way, consistent with an applied constant stressing rate.

(4) Using this new filtered modified stressing rate, run for a long time (hundreds of thousands of years).

(5) Measure the accumulated slip over this long run and divide by time to get slip rates on faults.

(6) Use this new empirical slip rate function as input to backslip loading. This is the new backslip-from-stress loading mode. This slip-rate function can be used for rupture parameters different from those than it was generated under, since it only depends on the cumulative slip, not the individual slip events.

## SUPPLEMENTARY MATERIALS

Supplementary material for this article is available at <http://advances.sciencemag.org/cgi/content/full/4/8/eaau0688/DC1>

Fig. S1. Map of difference in recurrence intervals in the earthquake simulator compared with UCERF3.

Fig. S2. Parameter sensitivity study.

Fig. S3. Parameter sensitivity study.

Fig. S4. Parameter sensitivity example showing the spatial structure of changes in hazard.

Fig. S5. Parameter sensitivity example showing the spatial structure of changes in hazard relative to UCERF3.

Fig. S6. Weak magnitude dependence of GMMS.

References (25–29)

## REFERENCES AND NOTES

1. C. A. Cornell, Engineering seismic risk analysis. *Bull. Seismol. Soc. Am.* **58**, 1583–1606 (1968).
2. E. H. Field, R. J. Arrowsmith, G. P. Biasi, P. Bird, T. E. Dawson, K. R. Felzer, D. D. Jackson, K. M. Johnson, T. H. Jordan, C. Madden, A. J. Michael, K. R. Milner, M. T. Page, T. Parsons, P. M. Powers, B. E. Shaw, W. R. Thatcher, R. J. Weldon II, Y. Zeng, Uniform California Earthquake Rupture Forecast, version 3 (UCERF3)—The time-independent model. *Bull. Seismol. Soc. Am.* **104**, 1122–1180 (2014).
3. K. Sieh, L. Jones, E. Haaksson, K. Hudnut, D. Eberhart-Phillips, T. Heaton, S. Hough, K. Hutton, H. Kanamori, A. Lilje, S. Lindvall, S. F. McGill, J. Mori, C. Rubin, J. Spotila, J. Stock, H. K. Thio, J. Trieman, B. Wernicke, J. Zachariasen, Near-field investigations of the Landers earthquake sequence, April to July 1992. *Science* **260**, 171–176 (1993).
4. Y. Klinger, X. W. Xu, P. Tapponnier, J. Van der Woerd, C. Lasserre, G. King, High-resolution satellite imagery mapping of the surface rupture and slip distribution of the M-w 7.8, 14 November 2001 Kokoxili earthquake, Kunlun Fault, Northern Tibet, China. *Bull. Seismol. Soc. Am.* **95**, 1970–1987 (2005).
5. D. Eberhart-Phillips, P. Haeussler, J. T. Freymueller, A. D. Frankel, C. M. Rubin, P. Craw, N. A. Ratchkovski, G. Anderson, G. A. Carver, A. J. Crone, T. E. Dawson, H. Fletcher, R. Hansen, E. L. Harp, R. A. Harris, D. P. Hill, S. Hreinsdóttir, R. W. Jibson, L. M. Jones,

R. Kayen, D. K. Keefer, C. F. Larsen, S. C. Moran, S. F. Personius, G. Plafker, B. Sherrod, K. Sieh, N. Sitar, W. K. Wallace, The 2002 Denali fault earthquake, Alaska: A large magnitude, slip-partitioned event. *Science* **300**, 1113–1118 (2003).

6. I. J. Hamling, S. Hreinsdóttir, K. Clark, J. Elliott, C. Liang, E. Fielding, N. Litchfield, P. Villamor, L. Wallace, T. J. Wright, E. D'Anastasio, S. Bannister, D. Burbidge, P. Denys, P. Gentle, J. Howarth, C. Mueller, N. Palmer, C. Pearson, W. Power, P. Barnes, D. J. A. Barrell, R. Van Dissen, R. Langridge, T. Little, A. Nicol, J. Pettinga, J. Rowland, M. Stirling, Complex multifault rupture during the 2016  $M_w$  7.8 Kaikōura earthquake, New Zealand. *Science* **356**, eaam7194 (2017).

7. H. Castaños, C. Lomnitz, PSHA: Is it science? *Eng. Geol.* **66**, 315–317 (2002).

8. S. Stein, R. J. Geller, M. Liu, Why earthquake hazard maps often fail and what to do about it. *Tectonophysics* **562–563**, 1–25 (2012).

9. F. Mulargia, P. B. Stark, R. J. Geller, Why is Probabilistic Seismic Hazard Analysis (PSHA) still used? *Phys. Earth Planet. Inter.* **264**, 63–75 (2017).

10. M. D. Petersen, M. P. Moschetti, P. M. Powers, C. S. Mueller, K. M. Haller, A. D. Frankel, Y. Zeng, S. Rezaeian, S. C. Harmsen, O. S. Boyd, N. Field, R. Chen, K. S. Rukstales, N. Lucco, R. L. Wheeler, R. A. Williams, A. H. Olsen, The 2014 United States national seismic hazard model. *Earthq. Spectra* **31**, S1–S30 (2015).

11. M. R. Munafò, G. Davey Smith, Repeating experiments is not enough. *Nature* **553**, 399–401 (2018).

12. E. H. Field, G. P. Biasi, P. Bird, T. E. Dawson, K. R. Felzer, D. D. Jackson, K. M. Johnson, T. H. Jordan, C. Madden, A. J. Michael, K. R. Milner, M. T. Page, T. Parsons, P. M. Powers, B. E. Shaw, W. R. Thatcher, R. J. Weldon II, Y. Zeng, Long-term, time-dependent probabilities for the Third Uniform California Earthquake Rupture Forecast (UCERF3). *Bull. Seismol. Soc. Am.* **105**, 511–543 (2015).

13. E. H. Field, K. R. Milner, J. L. Hardebeck, M. T. Page, N. van der Elst, T. H. Jordan, B. E. Shaw, M. J. Werner, A spatiotemporal clustering model for the Third Uniform California Earthquake Rupture Forecast (UCERF3-ETAS)—Toward an operational earthquake forecast. *Bull. Seismol. Soc. Am.* **107**, 1049–1081 (2017).

14. J. H. Dieterich, K. B. Richards-Dinger, Earthquake recurrence in simulated fault systems. *Pure Appl. Geophys.* **167**, 1087–1104 (2010).

15. K. Richards-Dinger, J. H. Dieterich, RSQSim earthquake simulator. *Seismol. Res. Lett.* **83**, 983–990 (2012).

16. B. E. Shaw, K. Richards-Dinger, J. H. Dieterich, Deterministic model of earthquake clustering shows reduced stress drops for nearby aftershocks. *Geophys. Res. Lett.* **42**, 9231–9238 (2015).

17. B. E. Shaw, Earthquake surface slip length data is fit by constant stress drop and is useful for seismic hazard analysis. *Bull. Seismol. Soc. Am.* **103**, 876–893 (2013).

18. E. H. Field, T. H. Jordan, C. A. Cornell, OpenSHA: A developing community-modeling environment for seismic hazard analysis. *Seismol. Res. Lett.* **74**, 406–419 (2003).

19. Y. Bozorgnia, N. A. Abrahamson, L. Al Atik, T. D. Ancheta, G. M. Atkinson, J. W. Baker, A. Baltay, D. M. Boore, K. W. Campbell, B. S.-J. Chiou, R. Darragh, S. Day, J. Donahue, R. W. Graves, N. Gregor, T. Hanks, I. M. Idriss, R. Kamai, T. Kishida, A. Kottke, S. A. Mahin, S. Rezaeian, B. Rowshandel, E. Seyhan, S. Shahi, T. Shantz, W. Silva, P. Spudich, J. P. Stewart, J. Watson-Lamprey, K. Wooddell, R. Youngs, NGA-West2 Research Project. *Earthq. Spectra* **30**, 973–987 (2014).

20. Building Seismic Safety Commission, *NEHRP (National Earthquake Hazards Reduction Program) Recommended Seismic Provisions for New Buildings and Other Structures*, FEMA P-750 (Federal Emergency Management Agency, 2009).

21. A. S. Baltay, T. C. Hanks, Understanding the magnitude dependence of PGA and PGV in NGA-West2 Data. *Bull. Seismol. Soc. Am.* **104**, 2851–2865 (2014).

22. F. Rolandone, R. Bürgmann, R. M. Nadeau, Time-dependent depth distribution of aftershocks: Implications for fault mechanics and crustal rheology. *Seismol. Res. Lett.* **73**, 229 (2002).

23. B. E. Shaw, S. G. Wesnousky, Slip-length scaling in large earthquakes: The role of deep penetrating slip below the seismogenic layer. *Bull. Seismol. Soc. Am.* **98**, 1633–1641 (2008).

24. B. E. Shaw, Self-organizing fault systems and self-organizing elastodynamic events on them: Geometry and the distribution of sizes of events. *Geophys. Res. Lett.* **31**, L17603 (2004).

25. K. R. Milner, M. T. Page, E. H. Field, T. Parsons, G. P. Biasi, B. E. Shaw, Defining the inversion rupture set using plausibility filters, *USGS Open File Report 2013–1165, Uniform California Earthquake Rupture Forecast Version 3 (UCERF3)—The Time-Independent Model, Appendix T* (2013).

26. S. G. Wesnousky, Predicting the endpoints of earthquake ruptures. *Nature* **444**, 358–360 (2006).

27. R. A. Harris, R. J. Archuleta, S. M. Day, Fault steps and the dynamic rupture process: 2-d numerical simulations of a spontaneously propagating shear fracture. *Geophys. Res. Lett.* **18**, 893–896 (1991).

28. B. E. Shaw, J. H. Dieterich, Probabilities for jumping fault segment stepovers. *Geophys. Res. Lett.* **34**, L01307 (2007).

29. D. M. Boore, G. M. Atkinson, Ground-motion prediction equations for the average horizontal component of PGA, PGV, and 5%-damped PSA at spectral periods between 0.01 s and 10.0 s. *Earthq. Spectra* **24**, 99–138 (2008).

#### Acknowledgments

**Funding:** This work was supported by the W.M. Keck Foundation, by NSF grants EAR-1135455 and EAR-1447094, and by the Southern California Earthquake Center (SCEC) under NSF Cooperative Agreement EAR-1033462 and USGS Cooperative Agreement G12AC20038. Computational resources were provided by NSF EAR-130035, the University of Southern California Center for High Performance Computing, the Blue Waters National Center for Supercomputing Applications, and Texas Advanced Computing Center (SCEC contribution number 8093). **Author contributions:** B.E.S. developed the simulator fault model and the hybrid loading technique, carried out and refined simulations, initiated and formulated recurrence interval and hazard comparisons, and wrote the manuscript. K.R.M. developed the code for turning simulator event output into hazard measures and collaborated with B.E.S. on hazard comparisons. E.H.F. led the UCERF project including UCERF fault model development and OpenSHA tools for hazard calculations. K.R.-D. developed the simulator code and platform. J.J.G. pursued locally tuned simulator studies, which prompted B.E.S. to develop locally untuned studies in response. J.H.D. conceived simulator approximations and collaborated with K.R.-D. to develop the simulator platform. T.H.J. built collaboration, raised funds for effort, and provided multiple comments that substantially improved the manuscript. **Competing interests:** The authors declare that they have no competing interests. **Data and materials availability:** Extensive materials are available for the UCERF3 model more generally at [www.wgcep.org/UCERF3](http://www.wgcep.org/UCERF3). Materials for the simulator are available upon request from the authors. All data needed to evaluate the conclusions in the paper are present in the paper and/or the Supplementary Materials. Additional data related to this paper may be requested from the authors.

Submitted 3 May 2018

Accepted 17 July 2018

Published 22 August 2018

10.1126/sciadv.aau0688

**Citation:** B. E. Shaw, K. R. Milner, E. H. Field, K. Richards-Dinger, J. J. Gilchrist, J. H. Dieterich, T. H. Jordan, A physics-based earthquake simulator replicates seismic hazard statistics across California. *Sci. Adv.* **4**, eaau0688 (2018).

## A physics-based earthquake simulator replicates seismic hazard statistics across California

Bruce E. Shaw, Kevin R. Milner, Edward H. Field, Keith Richards-Dinger, Jacquelyn J. Gilchrist, James H. Dieterich and Thomas H. Jordan

*Sci Adv* **4** (8), eaau0688.  
DOI: 10.1126/sciadv.aau0688

### ARTICLE TOOLS

<http://advances.sciencemag.org/content/4/8/eaau0688>

### SUPPLEMENTARY MATERIALS

<http://advances.sciencemag.org/content/suppl/2018/08/20/4.8.eaau0688.DC1>

### REFERENCES

This article cites 27 articles, 11 of which you can access for free  
<http://advances.sciencemag.org/content/4/8/eaau0688#BIBL>

### PERMISSIONS

<http://www.sciencemag.org/help/reprints-and-permissions>

Use of this article is subject to the [Terms of Service](#)